NANO LETTERS

2007
Vol. 7, No. 1
218−222

Intermediate-Band Solar Cells Employing Quantum Dots Embedded in an Energy Fence Barrier

Guodan Wei and Stephen R. Forrest*

Departments of Materials Science and Engineering, Electrical Engineering and Computer Science, and Physics, University of Michigan, Ann Arbor, Michigan 48109

Received November 1, 2006

ABSTRACT

Power efficiencies >60% have been predicted for idealized quantum dot (QD) intermediate band solar cells. This goal has not yet been realized, due in part to nonidealities that result in charge trapping followed by recombination of photocarriers in the QDs, and the lack of an optimal materials combination. To eliminate charge trapping, a p^+–i–n^+ cell employing QDs buried within a high band gap barrier layer is proposed and analyzed. The maximum solar power conversion efficiency under AM1.5 spectral radiation of an example GaAs-based photovoltaic cell employing 10–20 layers of InAs QDs surrounded by $Al_xGa_{1-x}As$ barriers in the junction built-in depletion region can be as high as 45%. Higher efficiencies are anticipated for InP-based cells. This represents a significant improvement over GaAs homojunction cells with maximum efficiencies of <25%.

Quantum dot (QD) intermediate band solar cells have been actively investigated in recent years since it has been asserted that such cells have the potential for realizing solar power conversion efficiencies >60%.[1] Indeed, low band gap energy QDs can generate multiple electron−hole pairs (excitons) by absorption of a single high-energy photon, leading, in principle, to quantum efficiencies in excess of 100%.[2,3] To expand the spectral response to longer wavelengths, narrow band gap QDs (e.g., InAs) need to be packed sufficiently close to form an intermediate energy band within the gap of the host matrix material (e.g., GaAs). However, the high concentration of strained QDs introduces a high charge density ($\sim 1 \times 10^{16}$ cm^{-3})[4] in the dot region, and photoexcited carriers (electron and hole) are rapidly captured by the self-assembled QDs. Consequently, the very high efficiencies predicted for QD intermediate band solar cells have not been realized, due in part to nonideal band structures that result in charge trapping followed by recombination of the photocarriers in the dots. In contrast to laser applications where fast carrier trapping is required,[5] photogenerated carriers must tunnel through, or be transported around the QDs to avoid trapping and recombination at these sites.

Theoretical models[6] confirm that for relatively short recombination times (~2 ns), QDs act primarily as recombination rather than as generation centers, resulting in a decrease in photocurrent with an increase in the number (N) of QD layers within the larger band gap semiconductor host. Partial filling of confined states in the dot region of intermediate band solar cells by Si δ-doping[7] of the host has shown limited success. Although these devices have photoresponse extended to longer wavelengths, they also exhibit a significantly reduced open circuit voltage (V_{oc}) compared to large band gap homojunction cells. Indeed, no improvement in power conversion efficiency over a homojunction GaAs cell has yet been reported. Here, we propose a new quantum-dot-in-a-fence (DFENCE) heterostructure that includes an $Al_xGa_{1-x}As$ energy barrier "fence" surrounding InAs QDs and wetting layers embedded in a GaAs homojunction. A model that includes nonideal charge recombination and leakage current effects (in contrast to previous, idealized calculations of QD solar cells[1]) is presented. Our models lead to a practical DFENCE heterostructure solar cell, exploiting the self-organized, archetype InAs/GaAs system. Calculations suggest that the DFENCE structure can have power conversion efficiencies for an AM1.5 solar spectrum as high as 45% in nonideal GaAs structures (compared with <25% for conventional homojunction GaAs cells) and can yield even higher efficiencies using the InAs/InP system.

The structure of the DFENCE heterostructure in Figure 1 includes multiple layers of QDs in the intrinsic region of a GaAs p^+−i−n^+ structure. The InAs dots are assumed to be sandwiched between two thin, high band gap $Al_xGa_{1-x}As$ barrier layers, which are, in turn, embedded in GaAs. The spatial distribution of InAs dots in the GaAs /$Al_xGa_{1-x}As$ barriers can be treated as a dense, periodically arranged array of cylinders with length l and radius R. The thickness, t, of the $Al_xGa_{1-x}As$ fence barrier is assumed to be $0.1R$, and the

10.1021/nl062564s CCC: $37.00 © 2007 American Chemical Society
Published on Web 12/02/2006

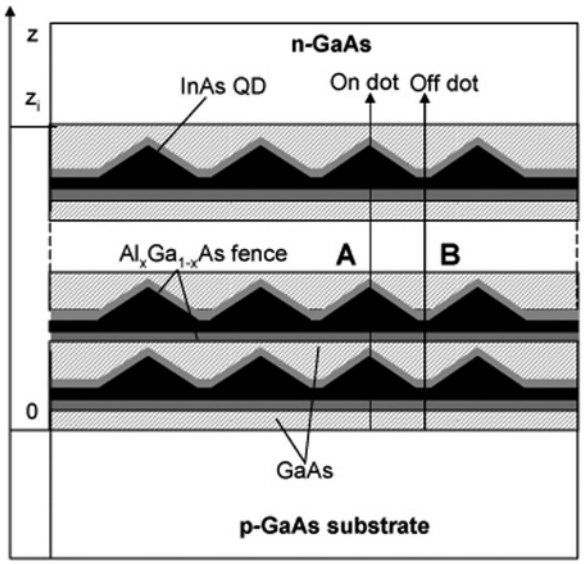

Figure 1. Structure of the quantum dots in a fence barrier (DFENCE) solar cell. Path A shows transport along on-dot sites through the GaAs buffer, $Al_xGa_{1-x}As$ fences, InAs wetting layers, and InAs quantum dots. Path B shows charge transport along off-dot sites through the GaAs buffer, InAs wetting layers, and $Al_xGa_{1-x}As$ fences.

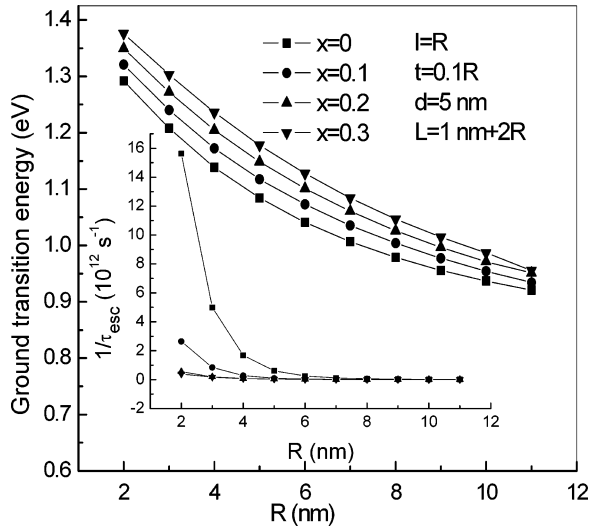

Figure 2. Ground state transition energy vs quantum dot radius of (R) with the thickness of fence barrier fixed to $t = 0.1R$ for Al fractions of $x = 0$, 0.1, 0.2, 0.3. Here, l is the dot length, d is the thickness of the surrounding GaAs layer, and L is the distance between quantum dots in the plane of the substrate surface. Inset: Carrier escape rate vs quantum dot radius.

thickness of the surrounding GaAs layer is d. The period for the QD "unit cell" is L parallel to the plane of the substrate surface, and $L_z = l + d + t$ normal to that surface. For determining the two-dimensional (2D) band structure, the conduction band offset between the strained InAs dot and GaAs buffer is 70% of their difference in band gaps (ΔE_{c1}),[8] and the conduction band offset between $Al_xGa_{1-x}As$ and GaAs is 67% of their band gap difference (ΔE_{c2}).[9] The electron and hole energy levels at the Γ point of periodic InAs/GaAs quantum dots buried in $Al_xGa_{1-x}As$ fence barriers along path A in Figure 1 are calculated by using the matrix elements determined through effective-mass envelope-function theory[10] for the QD with two finite barriers (fence barrier plus host layer).

As the QD size increases, the ground state photon transition energies decrease due to reduced confinement for the InAs/GaAs QD structure with or without the $Al_xGa_{1-x}As$ fences, as shown in Figure 2. The incorporation of an $Al_xGa_{1-x}As$ barrier layer ($x > 0$) surrounding the InAs QDs slightly increases the ground state photon transition energy due to the additional potential barrier of the fence. When $R = 8$ nm, the lowest transition energy in the absence of a fence is 1.06 eV, consistent with the absorption peak at 1.05 $\pm$ 0.05 eV observed in the luminescence of similar sized structures.[11] Hence, although the actual shape of InAs QDs approximates an equilateral tetrahedron, the approximation of the QD as a cylinder is adequate.

Once an electron−hole pair is photogenerated in the QD, it can either recombine or escape into the wide band gap host. After escape, the charges are separated by the built-in electric field of the junction and are collected at the electrodes. The competition between the recombination ($1/\tau_{rec}$) and the escape rates ($1/\tau_{esc}$) determines the photocurrent contributed by the QDs.[12] The escape rate is calculated based on two processes: direct tunneling through the trapezoidal fence barrier in the presence of the built-in electric field, and thermionic emission from the dot quantum state over the barrier. From the inset of Figure 2, the carrier escape rate decreases from 2.6×10^{12} to 3×10^{9} s^{-1} as both the localized energy level (defined as the difference between the QD state to the conduction band minimum of the GaAs barrier) and the activation energy[13] are increased with radii ranging from 2 to 11 nm when $x = 0.2$. When $R > 6$ nm, increasing the height of the barrier as controlled by increasing the Al fraction, x, does not lead to a significant change in escape rate as compared to the conventional case with no fence barriers (see inset, Figure 2).

The photocurrent density from the QDs is

$$j_D(z) = \int_{E_1}^{E_2} e \frac{G(E,z)}{1 + \tau_{esc}/\tau_{rec}} \, dE \tag{1}$$

with

$$J_D = \int_0^{z_i} j_D(z) \, dz \tag{2}$$

Here, e is the elementary charge, $G(E,z)$ is the photocarrier generation rate in the QDs within the i region,[14] and E_1 and E_2 are the lower and upper energies for absorption in the QDs, respectively. Also, z is the position in the i region (of total width, z_i) as measured from the metallurgical p−n junction, $j_D(z)$ is the incremental photocurrent generated at position z, and J_D is the total photocurrent collected from the N QD layers. The absorption coefficient of a QD is calculated based on the dipole transition matrix element between the conduction and valence band edge states using Fermi's golden rule.[15] Inhomogeneous Gaussian broadening of the photon transition energy contributes a width of

approximately 50 meV to the absorption spectrum.[11] For InAs QD systems, the radiative recombination time is typically $\tau_{rec} \sim 1$ ns,[12] as will be used in the subsequent analysis.

To understand the effect of the fence barrier on the charge transport properties along the on-dot (A) and off-dot (B) paths that include the presence of the InAs wetting layer[16,17] in Figure 1, we calculate the transmission coefficient as a function of the photocarrier and barrier energies based on the transfer matrix method, combined with the envelope function and effective mass approximations.[9] The average transmission coefficient, $\langle T \rangle$, characterizes the electron and hole tunneling efficiency through the fence without trapping into the discrete QD energy levels. The current is then equal to the number of carriers that tunnel along the on-dot paths, which, in turn equals the product of the tunneling probability and the number of carriers at that energy in the GaAs layers. Thus $\langle T \rangle$ can be expressed as

$$\langle T \rangle = \frac{\int_0^\infty N_c(E) f(E) T(E)\, dE}{\int_0^\infty N_c(E) f(E)\, dE} \tag{3}$$

where $N_c(E)$ is the GaAs conduction band density of states, $f(E)$ is the Fermi−Dirac distribution, and $T(E)$ is the transmission coefficient at incident electron energy, E. Along path A, $\langle T \rangle$ decreases from 65% with no fence barrier, to 25% (for $x = 0.1$) when the fence thickness increases from 0 to 1.6 nm. In contrast, along path B, $\langle T \rangle$ decreases from 24% (no fence barrier) to 12%. Although the conduction band offset (~0.33 eV[18]) between the InAs wetting layer and the GaAs buffer is comparable to that of the InAs QDs and the GaAs buffer (~0.513 eV), the extreme thinness of the wetting layer (≤2 nm[17]) results in a higher 2D ground state energy with few discrete energy levels between the fence barriers. Resonant tunneling from 3D to 0D states in the QDs contributes to their high $\langle T \rangle$. Hence, photocarriers predominantly tunnel through the QDs as a result of the thin fence barriers.

The reverse dark current density due to thermionic emission of electrons and holes from states in the InAs QDs and wetting layers is[19,20]

$$J_{DR} = e\upsilon N_{dot}\left[N_{cm}\sigma_e \exp\left(\frac{E_e - \Delta E_{c2} - E_c}{kT}\right) + N_{vm}\sigma_h \exp\left(-\frac{E_h + \Delta E_{v2} - E_v}{kT}\right)\right] \tag{4}$$

where N_{dot} is the area density of quantum dots (typically between 4.7×10^{10} and 5×10^{12} cm^{-2} for this material system[21]), N_{cm} and N_{vm} are the effective densities of electron and hole states in GaAs, E_c and E_v are the conduction and valence band energies of GaAs, E_e and E_h are the energy eigenvalues for electrons and holes in the InAs quantum dots (referenced to the conduction band edge of the InAs QDs), υ is the thermal velocity of electrons, σ_e and σ_h are the electron and hole capture cross sections, respectively, and ΔE_{v2} is the valence band offset between $Al_xGa_{1-x}As$ and GaAs. Also, the reverse saturation current, J_0, is reduced with an increase in band gap offset energy, ΔE, between GaAs and $Al_xGa_{1-x}As$ layers. Incorporating generation and recombination currents in both the GaAs layers and $Al_xGa_{1-x}As$ fence barriers yields

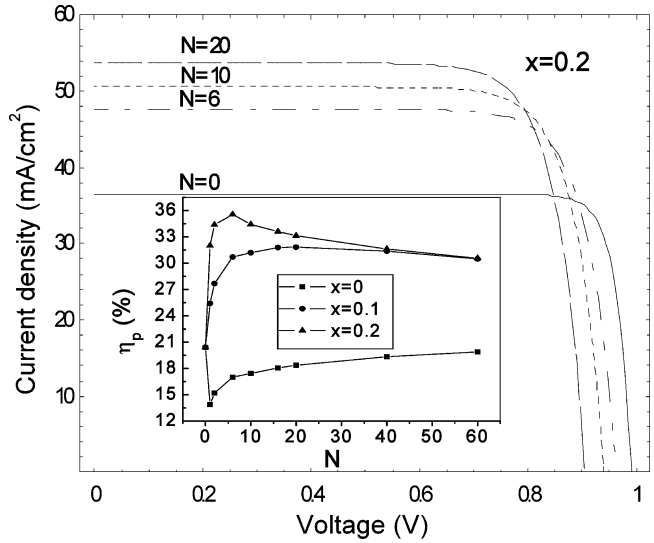

Figure 3. Current density vs voltage for GaAs DFENCE heterostructures as a function of the number of stacked quantum dot layers N ($x = 0.2$). Inset: power conversion efficiency vs number of qantum dot layers (N) for quantum dots with a radius of 8 nm when x increases from 0 to 0.2.

$$J = J_0 \exp\left(-\frac{\Delta E}{kT}\right)(1 + r_R\beta)\left[\exp\left(\frac{qV}{kT}\right) - 1\right] + [J_{NR} + J_s(N) + J_{DR}]\left[\exp\left(\frac{qV}{2kT}\right) - 1\right] - J_{sc} \tag{5}$$

where r_R is the fractional increase in the net i-region recombination at equilibrium due to the incorporation of the fence barrier, β is the ratio of the recombination current in the i-region at equilibrium to the reverse drift current resulting from minority carrier extraction, and J_{NR} is the nonradiative recombination current in the intrinsic GaAs regions.[22] Also, $J_s \propto N$ is the interface recombination current at the off-dot sites,[23] and J_{sc} is the short-circuit current density under illumination.

Solar cells employing a direct-gap semiconductor such as GaAs have close to 100% internal quantum efficiency and behave as temperature independent, constant-current sources proportional to the illumination intensity. The calculated current−voltage characteristics using eq 5 are shown for the QD intermediate band solar cells in Figure 3. In the absence of the QDs, the calculated open-circuit voltage, $V_{oc} = 1.01$ eV, is consistent with the experimental results for GaAs homojunction solar cells.[24] With an increase in the number of QD layers, J_{sc} increases for $x = 0.2$ as a result of absorption of the sub-GaAs-band gap photons, while V_{oc} is reduced only slightly from 1.01 eV ($N = 1$) to 0.91 eV ($N = 20$) due to recombination at GaAs/$Al_xGa_{1-x}As$ interfaces along path B and nonradiative recombination in the GaAs i-region.

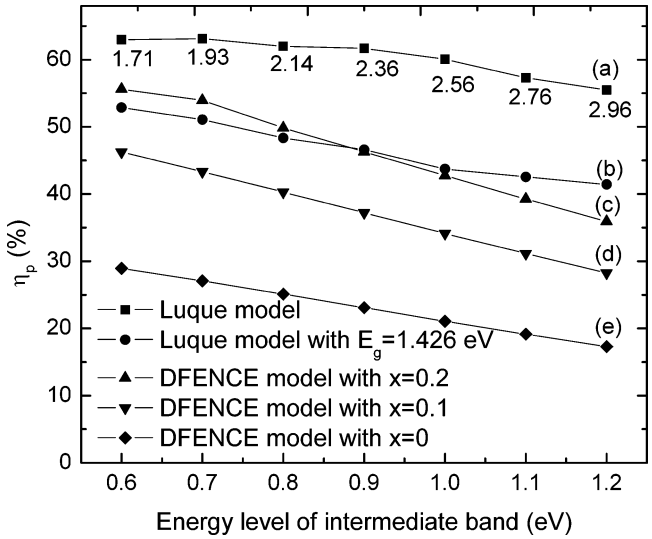

Figure 4. Power conversion efficiency vs intermediate band energy level calculated for (a) the ideal conditions proposed in ref 1 (Luque model), (b) the Luque model for GaAs with the band gap of 1. 426 eV, and (c−e) the upper limit of the DFENCE model with $x = 0.2$, 0.1, and 0. The labeled data in curve a is the bulk band gap assumed that corresponds with the intermediate band level on the abscissa to achieve maximum efficiency.

The calculated solar power conversion efficiency (η_P) for DFENCE cells under 1 sun (116 mW/cm^2), AM1.5 illumination, is shown in Figure 3, inset. Without the fence barrier ($x = 0$), V_{oc} decreases to 0.54 eV with an increase in the number (N) of stacked QD layers as a result of the large, thermally excited reverse saturation current ($J_{DR} \sim 10^{-5}$–10^{-6} A/cm^2) and nonradiative recombination in the InAs. Correspondingly, the power conversion efficiency is reduced from 20% (without QDs) to 15% in the QD cell. Hence, the power conversion efficiency is actually *reduced* in the QD intermediate band solar cells as proposed by Luque and Martí,[1] which is consistent with experimental results. In contrast, with the incorporation of $Al_xGa_{1-x}As$ fence (assuming $x = 0.1$−0.2), the power conversion efficiency can be as high as 36% with $N = 6$−20 QD layers and $R = 8$ nm due to the greatly reduced J_{DR}. When nonradiative recombination in the GaAs/$Al_xGa_{1-x}As$ layers dominates over generation in the QDs, η_P decreases with N. Due to competition between the absorption of sub-band-gap photons and recombination losses in the *i*-region, the optimal value of N is from 10 to 20. The greatly reduced reverse saturation current resulting from the incorporation of the $Al_xGa_{1-x}As$ fence, and increased short circuit current from the QDs, contributes to the enhanced power conversion efficiency.

The model of Luque et al.[1] predicts the maximum achievable power conversion efficiency of an ideal (i.e., no recombination or saturation current effects) hypothetical (i.e., independent of a specific materials combination) QD cell by choosing an optimal combination of intermediate quantum level and bulk band gap (curve a in Figure 4). Hence, to determine the performance of *practical* cells with realizable materials systems for comparison to the DFENCE architecture, it is necessary to calculate the corresponding maximum power conversion efficiency of GaAs/InAs-based QD intermediate band solar cells without fence barriers. The result of that calculation is shown by curve (b). In this case, the maximum η_P of GaAs-based intermediate band solar cells is 52%, with the intermediate band energy of between 0.6 and 0.7 eV, referenced to the valence band edge of GaAs.

Assuming that all incident photons with energies above the intermediate band level in the cell are absorbed in the intrinsic region of the DFENCE heterostructure, the upper limit for η_P with $N = 10$ approaches $\eta_P = 55\%$ of Luque et al. for an idealized QD structure whose intermediate band level is 0.6 eV (curve c, Figure 4); correspondingly, the ground state transition energy referenced to the discrete energy level of holes in InAs QDs should be 0.45 eV. Unfortunately, such a low ground state transition energy is not attainable due to the quantum confinement and large strain in the InAs dots (see Figure 2).

With an increase in intermediate band energy or ground state transition energy, the upper limit of the DFENCE structure efficiency decreases due to the concomitant reduction in sub-band-gap photocurrent. When the intermediate band energy is 1.2 eV (corresponding to the ground state transition energy of 1.05 eV in Figure 2), $\eta_P = 36\%$ ($x = 0.2$, curve c). The decrease of the potential barrier resulting from a decrease in Al concentration, x, results in decrease in η_P from 28% ($x = 0.1$, curve d) to 17% ($x = 0$, curve e) at the same intermediate band level of 1.2 eV. No significant enhancement in η_P for QD cells lacking a fence from curve e is observed in Figure 4. When the ground state photon transition energy is between 0.9 and 1.05 eV ($x = 0.2$, curve c), corresponding to an intermediate band level of between 1.05 and 1.20 eV, η_P of 35% to 45% is obtainable for $N \geq 10$.

Including the thin fence barriers surrounding QDs opens a new opportunity for narrowing the performance gap between high-performance multijunction solar cells and ideal intermediate band QD solar cells. There are several advantages to incorporating the energy barrier structure proposed here. (i) Resonant tunneling through on-dot and off-dot sites becomes possible by adjusting the height (via semiconductor alloy composition) and the thickness of the fence barrier without trapping in the QDs or wetting layers. (ii) The fences allow the QDs to function primarily as sub-band-gap photocarrier generation centers rather than as sites for undesirable recombination, without affecting V_{oc}. (iii) The reverse saturation current due to thermally generated minority carriers at the depletion layer edges and in the interior of the InAs layers is considerably reduced by the band gap offset between the fence and the narrow band gap host layers. With these properties, GaAs-based QD intermediate band DFENCE solar cells promise power conversion efficiencies as high as 45%. Heterostructures employing an energy fence can also be exploited in the InP-based materials system. In this case, the minimum transition energies in the InAs QDs can be as low as 0.65 eV,[25] corresponding to the energy that yields the maximum power conversion efficiency of nearly 55%, as shown in Figure 4.

Acknowledgment. We gratefully thank Kuen-Ting Shiu, Michael Logue, Marcelo Davanco, and Stephane Kená-

Cohen for helpful discussions and suggestions. We also acknowledge Global Photonic Energy Corporation for support of this work.

References

(1) Luque, A.; Marti, A. *Phys. Rev. Lett.* **1997**, *78*, 5014.
(2) Schaller, R. D.; Klimov, V. I *Phys. Rev. Lett.* **2004**, *92*, 186601−1.
(3) Philippe, G. S. *Nat. Mater*. **2005**, *4*, 653.
(4) Wetzler, R.; Wacker, A.; Schll, E.; Kapteyn, C. M. A.; Heitz, R.; Bimberg, D. *Appl. Phys. Lett*. **2000**, *77*, 1671.
(5) Asryan, L. V.; Suris, R. A. *Semicond. Sci. Technol*. **1996**, *11*, 554.
(6) Aroutiounian, V.; Petrosyan, S.; Khachatryan, A. *Sol. Energy Mater. Sol. Cells* **2005**, *89*, 165.
(7) Martí, A.; López, N.; Antolín, E.; Stanley, C.; Farmer, C.; Cuadra, L.; Luque, A. *Thin Solid Films* **2006**, *511*, 638.
(8) Colombelli, R.; Piazza, V.; Badolato, A.; Lazzarino, M.; Schoenfeld, F. B. W.; Petroff, P. *Appl. Phys. Lett*. **2000**, *76*, 1146.
(9) Harrison, P. *Quantum Well, Wires and Dots*; Wiley: England, 2005; p 459.
(10) Han, X. X.; Li, J. M.; Wu, J. J.; Cong, G. W.; Liu, X. L.; Zhu, Q. S.; Wang, Z. G. *J. Appl. Phys*. **2005**, *98*, 053703.
(11) Marzin, J. Y.; Gérard, J. M.; Izraë, A.; Barrier, D.; Bastard, G. *Phys. Rev. Lett*. **1994**, *73*, 716.
(12) Chang, W. H.; Hsu, T. M.; Huang, C. C.; Hsu, S. L.; Lai, C. Y. *Phys. Rev. B* **2000**, *62*, 6959.
(13) Fu, Y.; Engström, O. *J. Appl. Phys*. **2004**, *96*, 6477.
(14) Aroutiounian, V.; Petrosyan, S.; Khachatryan, A. *J. Appl. Phys*. **2001**, *89*, 2268.
(15) Datta, S. *Quantum Phenomena*; Addison Wesley: New York, 1989; p 233.
(16) Morris, D.; Deveaud, B.; Regreny, A.; Auvray, P. *Phys. Rev. B* **1993**, *47*, 6819.
(17) Suzuki, T. K.; Nomoto, K.; Taira, K.; Hase, I. *Jpn. J. Appl. Phys*. **1997**, *36*, 1917.
(18) Brandt, O.; Lage, H.; Ploog, K. *Phys. Rev. B* **1992**, *45*, 4217.
(19) Zhang, S. K.; Zhu, H. J.; Lu, F.; Jiang, Z. M.; Wang, X. *Phys. Rev. Lett*. **1998**, *80*, 3340.
(20) Engström, O.; Kaniewska, M.; Fu, Y.; Piscator, J.; Malmkvist, M. *Appl. Phys. Lett*. **2004**, *85*, 2908.
(21) Yeoh, T. S.; Liu, C. P.; Swint, R. B.; Huber, A. E.; Roh, S. D.; Woo, C. Y.; Lee, K. E.; Coleman, J. J. *Appl. Phys. Lett*. **2001**, *79*, 221.
(22) Anderson, N. G. *J. Appl. Phys*. **1995**, *78*, 1850.
(23) Rimada, J. C.; Hernandez, L.; Connolly, J. P.; Barnham, K. W. J. *Phys. Status Solidi* B **2005**, *242*, 1842.
(24) Tobin, S. P.; Vernon, S. M.; Bajgar, C.; Wojtczuk, S. J.; Melloch, M. R.; Keshavarzi, A.; Stellwag, T. B.; Venkatensan, S.; Lundstrom, M. S.; Emery, K. A. *IEEE Trans. Electron Devices* **1990**, *37*, 469.
(25) Holm, M.; Pistol. M. E.; Pryor, C. *J. Appl. Phys*. **2002**, *92*, 932.

NL062564S